Bi-functional Metasurface Polarizer for Reflected and Transmitted Waves

Xiaojun Huang (hxj@xust.edu.cn)
College of Communication and Information Engineering, Xi'an University of Science and Technology
Xia Ma
College of Communication and Information Engineering, Xi'an University of Science and Technology
Xuewen Li
College of Safety Science and Engineering, Xi'an University of Science and Technology
Jingdao Fan
College of Safety Science and Engineering, Xi'an University of Science and Technology
Liang Guo
College of Physics and Electrical Engineering, Kashi University
Helin Yang
College of Physical Science and Technology, Central China Normal University

Research Article

Keywords: Metasurface Polarizer, Reflected and Transmitted Waves

Posted Date: September 29th, 2021

DOI: https://doi.org/10.21203/rs.3.rs-936537/v1

Bi-functional metasurface polarizer for reflected and transmitted waves

Xiaojun Huang[1*], Xia Ma[1], Xuewen Li[2], Jingdao Fan[2], Liang Guo[3], Helin Yang[4*]

[1] College of Communication & Information Engineering, Xi'an University of Science and Technology, Xi'an, 710054

[2] College of Safety Science and Engineering, Xi'an University of Science and Technology, Xi'an, Shaanxi, 710054, China

[3]College of Physics and Electrical Engineering, Kashi University, Kashi 844007, China

[4]College of Physical Science and Technology, Central China Normal University, Wuhan 430079

Corresponding author: Xiaojun Huang hxj@xust.edu.cn

Helin Yang emyang@mail.ccnu.edu.cn

Abstract

Manipulating the polarizations of electromagnetic waves by flexible and diverse means is desirable for a myriad of microwave systems. More recently, metasurfaces offer the promising alternatives to conventional polarization manipulating components because of the flexibility of their geometry could be arbitrarily customized. In this context, a bi-layered metasurface was presented to simultaneously manipulate the polarized states of reflected and transmitted microwaves. No matter whether the incident electromagnetic wave is x-polarized or y-polarized, the reflected and transmitted waves will be converted into orthogonal y- polarized waves at the operating frequency. The designed metasurface has a high polarization conversion

rate(PCR) above 90% for both normal and oblique incidence. The experimental results verify the correctness of the simulated results. Finally, axial ratio and surface current distributions were employed to reveal the physics of polarization manipulation. The proposed metasurface will be beneficial to the design of flexible and versatile polarization converters and has great potential for applications in polarization controlled devices and also is believed extendable to higher frequency regimes.

Introduction

The polarization of electromagnetic (EM) wave is crucial in electromagnetic wave propagation, which has aroused increasing attention and interest, especially in the visible spectrum[1–3]. How to regulate the polarization form of EM wave in the process of propagation optionally is an essential and persistent research hotspot, which has fascinating application prospects from microwave to visible light[4–8], such as spectroscopic analysis[9,10], sensing[11,12], and polarization imaging[13]. Conventional approaches to manipulate the polarization state of light using birefringent crystals and grating structures are subject to bulky waveplates[14–16], thus the inherent defects of the conventional polarizers are large geometry and low efficiency in natural materials, which are difficult to meet in the current miniaturization of microwave and optical system integration. Metamaterials (MMs) are artificially engineered planar materials that typically with sub-wavelength periodic structures[17,18], which exhibit EM properties not existed in nature, such as negative refraction[19,20], perfect absorbers[17,21], and electromagnetic cloaking[22,23]. Metasurface (MS) is a kind of two-dimensional MM, which not only possesses the exotic EM characteristics not existed in nature

metamaterials, but also has the advantages of design, fabrication and integration compared to the MMs.

In recent years, MS offers the promising alternatives to conventional polarization manipulating devices due to its extreme wavefront and low-profile polarization control characteristics[2]. A myriad of MS-based polarization conversion devices with various of structures including typical SSR unit have been proposed theoretically and experimentally ranging from microwave to optical frequencies, such as multi-band or broadband linearly orthogonal polarization conversion in reflection or transmission EM waves[24–27], circularly cross-polarization converters[28,29], linear-circular polarization conversion[30-32]. Hao et al. reported an I-shaped structure achieving the 90° polarization rotation in reflection mode with high efficiency conversion ratio at two different frequencies for linearly polarized waves working in microwave frequency[33]. Subsequently, a broadband reflection cross-polarization conversion was realized using cur-wire MSs in microwave and terahertz frequency bands[34–36]. Additionally, a novel metallic helical MMs were introduced as polarizers with the properties of asymmetric, broadband circular-polarization conversion[37]. Various structures are used to achieve highly efficient and multi-band MM-based linear to circular polarization conversion, such as SRRs[38,39], Q-shaped[40] and twisted Hilbert-shaped chiral MSs [41]. Although MS-based polarization conversion devices have dramatically enhanced the bandwidth and efficiency compared to the conventional polarization filter, one crux issue of MSs-based polarization conversion in previous contributions is the independency of reflected and transmitted waves. The

polarization states can be manipulated with the MS converters of the reflected waves without considering the transmission process since the metallic ground plane can block the transmission of EM waves. In addition, the transmitted polarization converters can also convert the transmitted EM waves while the reflected EM waves were neglected. Therefore, simultaneous manipulating of reflected and transmitted waves in different polarized modes illumination is still a problem in the practical applications.

In this paper, a two-layer MS based on typical split ring resonators (SRRs) is numerically and experimentally demonstrated manipulating the polarization states of both reflected and transmitted waves. The results exhibits that either x- or y-polarized waves normally incidence are reflected and transmitted into their orthogonal components across the proposed MS. The proposed MS has a high PCR above 90% at both normal and oblique incidence. For an x-polarized incident wave, the MS will convert the reflected wave into a y-polarized wave at f_1 = 3.76 GHz and f_2 = 9.74 GHz and also can convert the transmitted wave into y-polarized wave at f_1 = 3.36 GHz, f_2 = 7.66 GHz, and f_3 = 11.25 GHz, respectively. When a y-polarized wave is incident, the reflected wave can be converted into x-polarized wave at f_1 = 4.64 GHz and f_2 = 11.25 GHz and the transmitted wave can be converted into x-polarized wave at f_1 = 4.19 GHz, f_2 = 7.78 GHz, and f_3 = 13.19 GHz, respectively. More importantly, the performance of angular tolerance will improve the device's performance against the incidence and reduce the requirements of optical components in the system. The designed MS has the potential applications in EM polarization control and stealth

systems.

Design and characteristics

Figure 1 shows the designed structure, and it consists of two identical typical split rings separated by a substrate lamina. The top layer is shown in Figure 1(a), the gap of the split ring is cut along the middle line between the x-axis and the y-axis. As shown in Figure 1(b), the angle (2β) of two gaps between the top layer and bottom layer is 90°. The substrate lamina is F4B with the thickness of 1 mm, the complex permittivity is 2.65 with a dielectric loss tangent of 0.001. The split ring is made of copper with the thickness 0.035mm and the conductivity of 5.8×10^7 S/m.

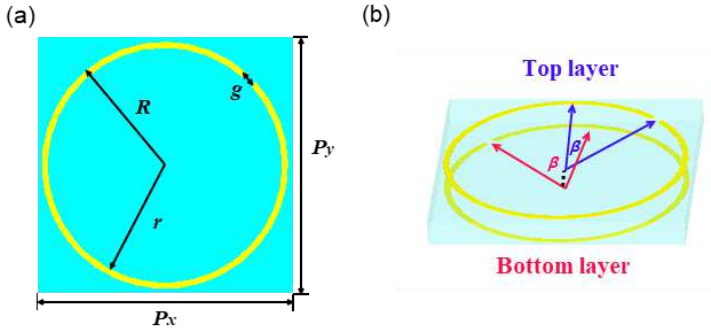

Figure 1. (a) The front view of structure in *xoy* plane. The top layer of copper SRR inlaid on the F4B substrate, the specific geometrical parameters of the structure are R = 4.8 mm, r = 4.56 mm, g = 0.4 mm, $P_x = P_y$ = 10 mm. (b) scenogram of the structure, the two identical copper layers are rotated the angle of 2β relatively, and $\beta = 45°$ in the simulations.

Figure 2 shows the operating principle of the polarization conversion for the proposed MS. Such a simple MS can provide dual-polarization manipulation of reflected and transmitted waves simultaneously. As shown in Figure 2, when the

x-polarized waves incident into the designed MS, it can be converted into y-polarized waves in the reflection mode, while the x-polarized waves can be converted into their y- polarized waves in the transmission mode. The y-polarized wave can be converted into its orthogonal polarized wave in the reflection mode when the x-polarized wave incidents into the designed MS, and simultaneously be transformed the y-polarized wave into x- polarized wave in the transmission case. The above working processes will demonstrate that the designed MS can simultaneously regulate the reflected wave and transmitted wave with different functionalities.

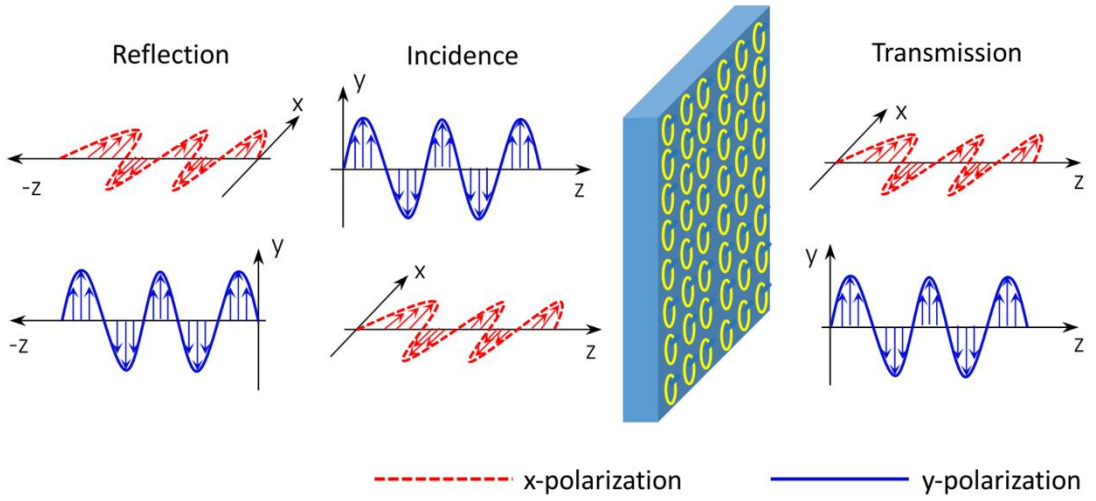

Figure 2. Operating principle diagram of the polarization conversion for the proposed MS. The x-polarization incidence can be reflected and transmitted in the form of y-polarized wave at the working frequencies, and y-polarization can be reflected and transmitted into x-polarization wave at the working frequencies. That is, the reflected wave and transmitted wave will be converted into their orthogonal waves at the working frequencies. Red dotted line indicates x-polarization wave, and blue real line indicates y-polarization wave.

Results and Discussion

Firstly, we define the reflection matrix $\boldsymbol{R}$ and transmission matrix $\boldsymbol{T}$ as[42]:

$$\boldsymbol{R} = \begin{pmatrix} \boldsymbol{r}_{xx} & \boldsymbol{r}_{xy} \\ \boldsymbol{r}_{yx} & \boldsymbol{r}_{yy} \end{pmatrix}, \quad \boldsymbol{T} = \begin{pmatrix} \boldsymbol{t}_{xx} & \boldsymbol{t}_{xy} \\ \boldsymbol{t}_{yx} & \boldsymbol{t}_{yy} \end{pmatrix} \tag{1}$$

Herein, x and y represent x- and y-polarized wave, respectively. r_{xx} and r_{yx} represent the reflectance of co-polarization and cross-polarization when x-polarized wave incidents into the MS, respectively. r_{yy} and r_{xy} represent the reflectance of co-polarization and cross-polarization when y-polarized waves incident to the MS, respectively. Correspondingly, the transmitted waves are defined in the same way. PCR is used to reveal the polarization conversion performance of the proposed MS, which can be defined as[33,43]:

$$\text{Reflection: } \mathrm{PCR}_x = \frac{r_{yx}^{\,2}}{r_{yx}^{\,2} + r_{xx}^{\,2}}, \quad \mathrm{PCR}_y = \frac{r_{xy}^{\,2}}{r_{xy}^{\,2} + r_{yy}^{\,2}} \tag{2}$$

$$\text{Transmission: } \mathrm{PCR}_x = \frac{t_{yx}^{\,2}}{t_{yx}^{\,2} + t_{xx}^{\,2}}, \quad \mathrm{PCR}_y = \frac{t_{xy}^{\,2}}{t_{xy}^{\,2} + t_{yy}^{\,2}} \tag{3}$$

Herein, the transmittance is not considered when calculating PCR of reflection polarization, and similarly, the reflectance is also neglected when calculating PCR of transmission polarization. The advantage of which is that we can obtain the energy conversion of reflected and transmitted wave independently. The polarization azimuth rotation angle Ψ can be calculated by the following formula[43,44]:

$$\Psi = \frac{1}{2}\operatorname{atan}\frac{2p\cos\varphi}{1 - p^2} \tag{4}$$

Where $p = r_{ij} / r_{jj}$ or $p = t_{ij} / t_{jj}$, φ represents the phase difference between the cross-polarization coefficient and co-polarization coefficient in reflection or

transmission cases.

Figure 3 depicts the simulated and experimental reflectance under x-polarized wave incidence. It shows in Figure 3(a) and 3(b) that r_{xx} is 0.02 and 0.01 and r_{yx} is 0.09 and 0.41 at f_1 = 3.76 GHz and f_2 = 9.74 GHz, respectively. We can see from Figure 3(b,c), r_{yx} of the converted y-polarized wave is slightly low, but PCR is larger than 0.9 at f_1 = 3.76 GHz, which means that more than 90% of the reflected energy has already been converted into y-polarized wave. The polarization azimuth rotation angle Ψ calculated from the simulation and experimental results are shown in Figure 3(d). It exhibits that Ψ under x-polarized incident wave are 73.4° and 75.6° at f_1 =3.76 GHz and f_2 =9.74 GHz, respectively. This means the polarization angle of reflected wave is rotated by 73.4° and 75.6° relative to the incident wave. It can be seen that the experimental results verified the correctness of the simulation results. Specifically, the cross-polarization reflection coefficient in the experiment is significantly different from that in the simulation, and the experimental result is larger than that in the simulation at 2-9 GHz, this error is generated during the experiment and is inevitable in the experiment, which is explained in detail in the experimental section.

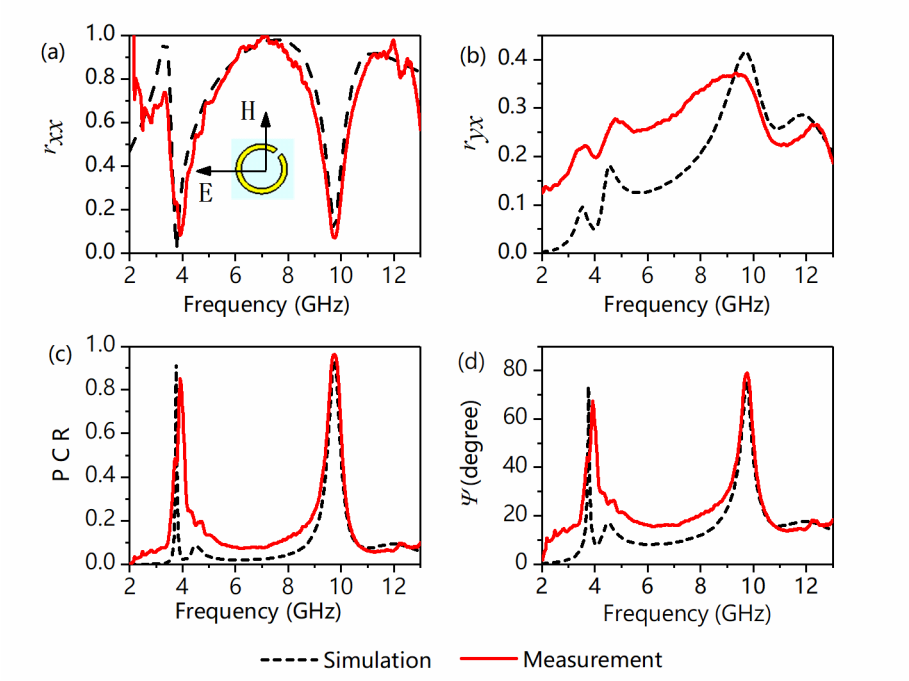

Figure 3. (a) co-polarization reflectance of r_{xx}, (b)cross-polarization reflectance of r_{yx}, (c) polarization conversion ratio (PCR), (d) polarization rotation angle of Ψ. The inset of Figure 3(a) depicts the orientation of the fields with respect to the structure, i.e. the directions of E-field and H-field along x and y axis, respectively.

Figure 4 shows the simulated and experimental results of transmission when x-polarization incident. We can see from Figure 4(a,b) that t_{xx} is approaching zero and t_{yx} is about 0.05, 0.04, and 0.28 at f_1 = 3.36 GHz, f_2 = 7.66 GHz, and f_3 = 11.25 GHz, respectively. PCR is larger than 0.8 and Ψ is larger than 75° at these three frequencies, which is in Figure 4(c,d). Therefore, it is proved that the transmitted wave is nearly converted into its orthogonal component through the designed MS.

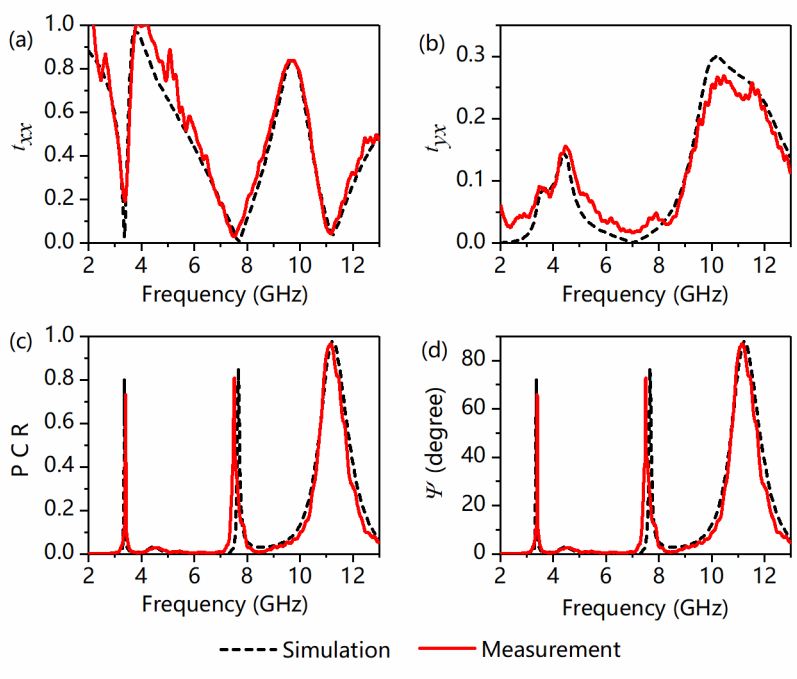

Figure 4. (a) co-polarization transmittance of t_{xx}, (b)cross-polarization transmittance of t_{yx}, (c) polarization conversion ratio (PCR), (d) polarization rotation angle of Ψ.

In what follows, we consider the polarization properties of designed MS under y-polarized wave incidence. From Figure 5(a,b), we can see that r_{yy} are 0.04 and 0.06 at f_1 = 4.64 GHz and f_2 = 11.25 GHz, r_{xy} are 0.19 and 0.27 at these two frequencies, respectively. Accordingly, PCR and Ψ are calculated and shown in Figure 5(c,d), we can see that PCR is greater than 0.95 at f_1 = 4.64 GHz and f_2 = 11.25 GHz, and Ψ of y-polarized incident wave are 75.9°and 77.4°at these two frequencies, respectively. The simulated and experimental transmission spectra under y-polarization normally incidence is shown in Figure 6. We can see that t_{yy} is almost totally 0 while t_{xy} is existed at f_1 = 4.20 GHz, f_2 = 7.78 GHz, and f_3 = 13.17 GHz, respectively. These above results demonstrate that the polarization conversion is realized in these three frequencies. As shown in Figure 6(c,d), PCR and Ψ under y-polarized wave incidence

confirmed that the MS can convert the incident wave into its cross-component wave at 4.20 GHz, 7.78 GHz, and 13.17 GHz, respectively.

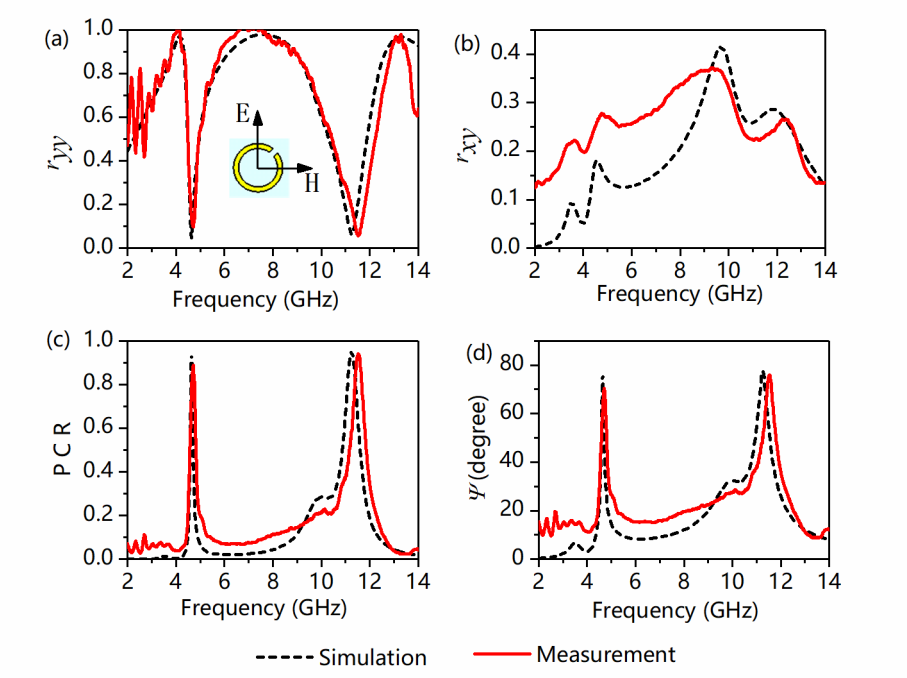

Figure 5. Results of reflected wave under y-polarized wave incidence. The inset of Figure 5(a) depicts the orientation of the fields with respect to the structure, i.e. the directions of H-field and E-field along x and y axis, respectively. (a) co-polarization reflectance of r_{yy}, (b)cross-polarization reflectance of r_{xy}, (c) polarization conversion ratio (PCR), (d) polarization rotation angle of Ψ.

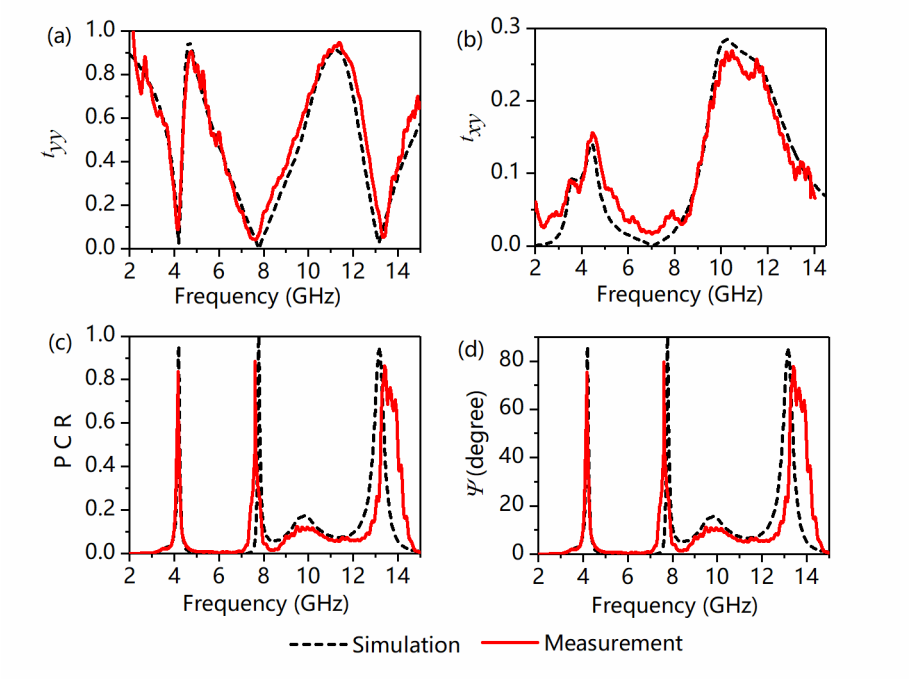

Figure 6. (a) co-polarization transmittance of t_{yy}, (b)cross-polarization transmittance of t_{xy}, (c) polarization conversion ratio (PCR), (d) polarization rotation angle of Ψ.

The superiority of the designed MS is that, it can work in a wide oblique incident angle. Figure 7 shows the PCR at different incident angles ranging from 0°to 60°with the step of 15°. We can see from Figure 7(a, b) that under the x-polarized incident wave, when the incident Angle increases to 60°, PCR is almost unaffected in either reflection mode or transmission mode. However, the PCR both in reflection and transmission modes are decreased monotonically when the incident angle increased from 0° to 60° under y-polarization incident wave shown in Figure 7(c,d). Specifically, the PCR is decreased with increasing the incident angle from 0°to 60° under x-polarization incidence at 3.36 GHz and 7.67 GHz, which is owing to the transmittance at these two frequencies is so smaller that the slight deviation can cause the change. This phenomenon is not appeared under y-polarization incidence, the

reason of which is that the response of magnetic coupling between two layers is in the waning for y-polarization. For x-polarization incidence, the direction of magnetic field along y-axis, which can stimulate the circular currents effectively at the arbitrary oblique incident angles. On the contrary, in the case of y-polarization incidence, the magnetic field is along x-axis, and the magnetic field is uncapable of exciting the circular currents effectively at the arbitrary oblique incident angles[44]. To allow a better view of the polarization conversion effect, the axial ratio is shown in Figure 8. The value of axial ratios is 4.59 dB at 3.76 GHz, 11.31 dB at 9.74 GHz, 6.18 dB at 3.36 GHz, 11.72 dB at 7.66 GHz, 12.30 dB at 11.25 GHz for x-polarization incidence, respectively; 11.79 dB at 4.64 GHz, 9.84 dB at 11.25 GHz, 10.99 dB at 4.19 GHz, 14.20 dB at 7.78 GHz, 12.38 dB at 13.17 GHz for y-polarization incidence, respectively. We can see that the axial ratio is nearly higher than 5 dB at the resonant frequencies where the PCR is almost larger than 90%.

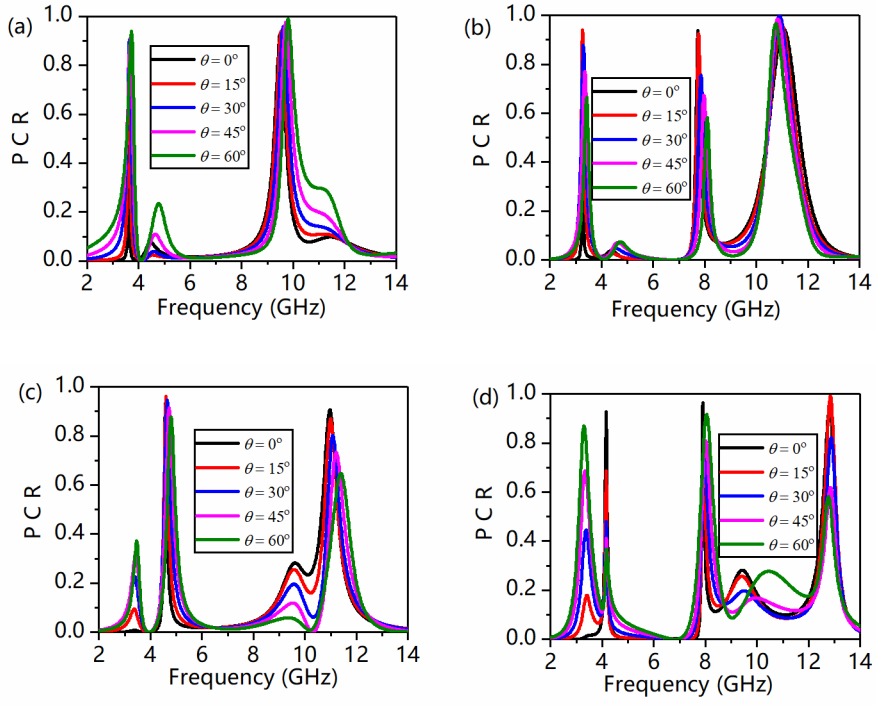

Figure 7. (a) PCR of reflection under x-polarization, (b) PCR of transmission under x-polarization, (c) PCR of reflection under y-polarization. (d) PCR of transmission wave under y-polarization.

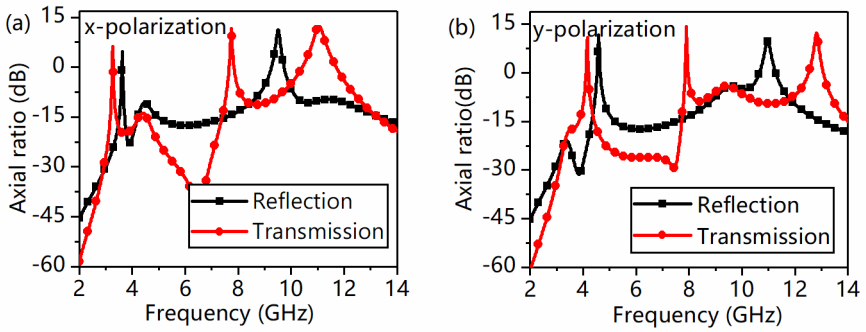

Figure 8. Axial ratio of the cross-polarization to co-polarization, (a) the axial ration of reflection and transmission in x-polarization incident. (b) the axial ration of reflection and transmission in y-polarization incident.

Herein, the physics of polarization conversion is investigated by using surface current distributions. We depict the surface current distributions in Figure 9, and taking the y-polarized wave as an example. Figure 9(a) shows the surface current distribution at 4.64 GHz, we can see from the figure that the magnetic dipole is excited along the y- axis, thus the electric field correspondingly along the x axis, it means that the MS converts y-polarized wave into x-polarized wave at 4.64 GHz under the reflected situation. Compared with the frequency of 1.64 GHz, two magnetic dipoles along the y direction are excited at 11.25 GHz shown in Fig 9(b), it is also indicated that the incident y-polarized wave is converted into x-polarized wave. For the transmitted wave, the surface current distributions at three resonant

frequencies along z- axis are shown in Figure 9(c-e). The excited magnetic fields come from the surface current mainly along the y axis, which indicates that the incident y-polarized wave is converted into x-polarized wave after transmission at the three resonant points. The difference is that as the frequency increases, the number of excited magnetic dipoles gradually increases. It is well understood from the transmission line theory that as the resonant frequency increases, the capacitance and inductance that generate resonance decrease, and the corresponding current loop that forms magnetic dipole gradually decreases.

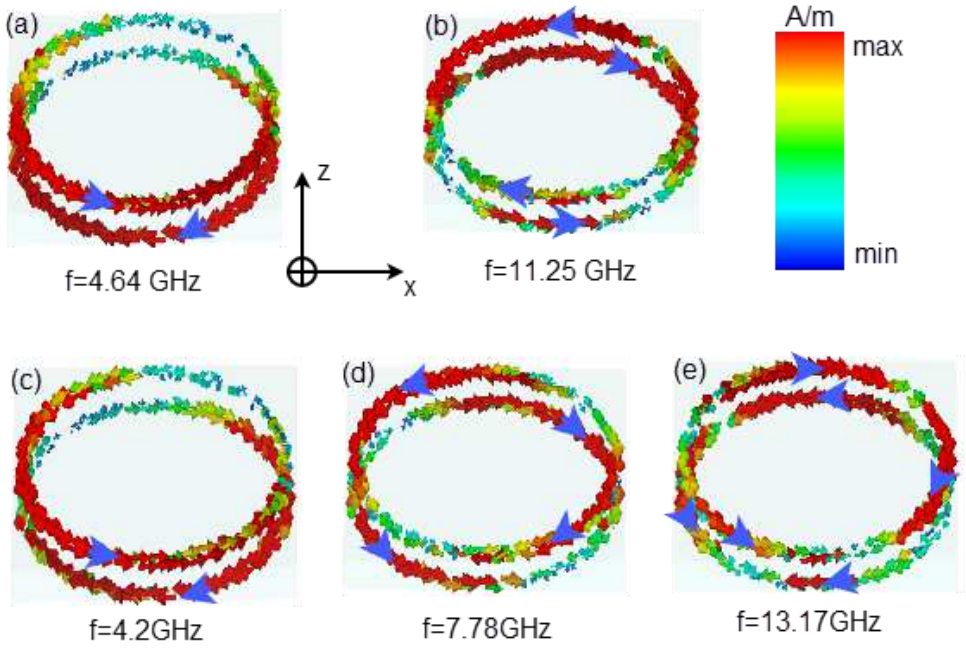

Figure 9. Surface current distributions. (a) and (b) are the reflected polarization resonances, and (c) (d) (e) are the transmitted polarization resonances.

Conclusion

In conclusion, we have demonstrated the design and experimental characteristics of

a bi-layered metasurface with polarization conversion of reflection wave and transmission wave. The designed metasurface can easily convert both the reflected wave and transmitted wave of x- and y-polarized into their orthogonal counterparts. The simulation results show that PCR is greater than 90% both in x- and y-polarization. The measured results performed by microwave experiments verified the simulated results. The proposed device has potential applications in many fields related to polarization manipulation. Multiple layers and different structures could be investigated in the future research, which has potential to provide improved bandwidth and efficiency.

Methods

The numerical simulations were calculated by CST MICROWAVE STUDIO. The unit cell boundary conditions are applied in x and y directions to mimic infinite boundaries; open (add space) boundary condition is set in z direction for representing the prpagation of EM waves. The port number of floquet modes was settled as 2 for both TE (x-polarization) and TM (y-polarization) waves, thus the reflection and transmission parameters of co- and cross-polarization can be calculated simultaneously.

For the measurement, the metasurface was fabricated with the identical geometry in the simulations employing standard printed circuit board (PCB) technology，the experiment sample is shown in figure 10(a). The reflection and transmission parameters were measured by a couple of identical standard broadband horn antennas (1-18 GHz) connected to the vector network analyzer (Agilent E8362B) via cables in

the anechoic chamber as showing in Figure 10(b,c). For measuring the reflection coefficients, the sample was placed in on the same side of two horns, and a copper plate with the same size of the sample was used for normalization. Horn 1 was firstly fixed with horizontal direction to emit y-polarized wave which will be reflected, and horn 2 was placed with horizontal and vertical direction to receive the reflected wave with co- and cross- polarization reflection coefficients; then horn 1 was rotated to vertical direction to emit x-polarized wave, and horn 2 received co- and cross-polarized wave in the same way. The distance between antennas and sample was 2 m to avoid the near field effect. A metal plate with the same size of the sample was used for calibration before the test. For measuring the transmission coefficients, the convertor was placed in the middle of the two horns, the co- and cross-polarization transmittances with different polarizations can be tested by rotating the direction of the two antennas. Herein, we have to mention that the disparity of the cross-polarization coefficient between simulation and experiment was caused the inherent setting experimental platform, especially for the cross-polarization reflection coefficients. The cross-polarization coefficient was tested through rotating the receiving antenna by 90° after calibration by a co-polarization antenna, thus the value to the calibration is slightly different when we rotated the antenna due to the inevitable change of incident angle and the center position of the receiving antenna.

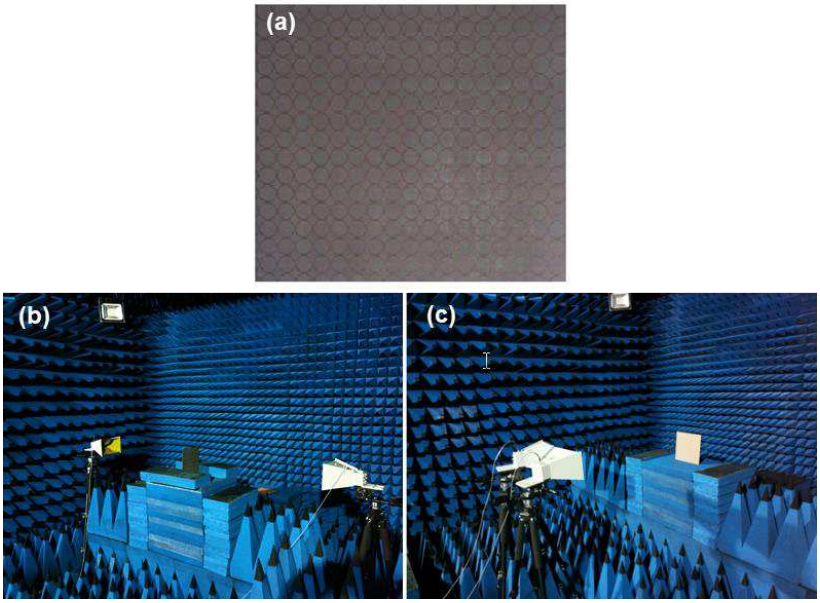

Figure 10. (a) Photograph of the fabricated sample;(b,c) Photograph of the experimental environment.

Acknowledgement

This work was supported by the Project of Science and Technology of Shaanxi Province (No.2019JLZ-08, 2021JM-395), the Science and Technology Plan Project of Xi'an Beilin District (No. GX1926), Natural Science Foundation of Xinjiang Uygur Autonomous Region (No.2018D01B01)

Author Contributions

X. H. and H. Y. conceived the idea and wrote the main manuscript text. X. H. and X. M. carried out the numerical calculations and experimental measurements. X. L. and J. F. analyzed and discussed the results. L. G. reviewed the manuscript and discussed the results. All authors contributed to scientific discussions about and critical revisions of the article.

Additional Information

Competing interests: The authors declare no competing interests.

References

1. Xu, P., Tian, H. W., Cai, X., Jiang, W. X. & Cui, T. J. Radiation-Type Metasurfaces for Advanced Electromagnetic Manipulation. *Adv. Funct. Mater.* **31**, 2100569 (2021).
2. Zhang, Y., Yang, L., Li, X. K., Wang, Y. L. & Huang, C. P. Dual Functionality of a Single-Layer Metasurface: Polarization Rotator and Polarizer. *J. Opt.* **22**, 035101 (2020).
3. Zhang, L., Mei, S., Huang, K. & Qiu, C. W. Advances in Full Control of Electromagnetic Waves with Metasurfaces. *Adv. Opt. Mater.* **4**, 818–833 (2016).
4. Zhang, K. *et al.* Polarization-Engineered Noninterleaved Metasurface for Integer and Fractional Orbital Angular Momentum Multiplexing. *Laser Photonics Rev.* **15**, 2000351 (2021).
5. Ding, G. *et al.* Independent Energy Allocation of Dual-Helical Multi-Beams with Spin-Selective Transmissive Metasurface. *Adv. Opt. Mater.* **8**, 2000342 (2020).
6. Lin, H., Lin, K. Te, Yang, T. & Jia, B. Graphene Multilayer Photonic Metamaterials: Fundamentals and Applications. *Adv. Mater. Technol.* **6**, 2000963 (2021).
7. Huo, P., Zhang, S., Liang, Y., Lu, Y. & Xu, T. Hyperbolic Metamaterials and

Metasurfaces: Fundamentals and Applications. *Adv. Opt. Mater.* **7**, 1801616 (2019).

8. Fedotov, V. A. *et al.* Dynamical Manipulation of Electromagnetic Polarization Using Anisotropic Meta-Mirror. *Science (80-.).* **6**, 30771- (2016).
9. Fedotov, V. A. *et al.* Asymmetric Propagation of Electromagnetic Waves through a Planar Chiral Structure. *Phys. Rev. Lett.* **97**, 167401 (2006).
10. Zhao, J., Zhang, J., Zhu, Z. & Yuan, X. Tunable Asymmetric Transmission of THz Wave Through a Graphene Chiral Metasurface. *J. Opt.* **18**, 095001 (2016).
11. Yoo, S. J. & Park, Q. H. Metamaterials and Chiral Sensing: A Review of Fundamentals and Applications. *Nanophotonics* **8**, 249–261 (2019).
12. Lee, Y. Y., Kim, R. M., Im, S. W., Balamurugan, M. & Nam, K. T. Plasmonic Metamaterials for Chiral Sensing Applications. *Nanoscale* **12**, 58–66 (2020).
13. John A. Montoya, Zhao-Bing Tian, Sanjay Krishna, and W. J. P. Ultra-Thin Infrared Metamaterial Detector for Multicolor Imaging Applications. *Opt. Express* **25**, 23343 (2017).
14. Wiesauer, K. & Jördens, C. Recent Advances in Birefringence Studies at THz Frequencies. *J. Infrared, Millimeter, Terahertz Waves* **34**, 663–681 (2013).
15. Broer, D. J., Lub, J. & Mol, G. N. Wide-Band Reflective Polarizers from Cholesteric Polymer Networks with a Pitch Gradient. *Nature* **378**, 467–469 (1995).
16. Smith, D. R., Pendry, J. B. & Wiltshire, M. C. K. Metamaterials and Negative Refractive Index. *Science (80-.).* **305**, 788–792 (2015).

17. Lin, H. *et al.* A 90-nm-Thick Graphene Metamaterial for Strong and Extremely Broadband Absorption of Unpolarized Light. *Nat. Photonics* **13**, 270 (2019).

18. Baryshnikova, K. V, Smirnova, D. A., Luk, B. S. & Kivshar, Y. S. Optical Anapoles : Concepts and Applications. *Adv. Opt. Mater.* **7**, 1801350 (2019).

19. Wang, W., Bonello, B., Djafari-rouhani, B., Pennec, Y. & Zhao, J. Double-Negative Pillared Elastic Metamaterial. *Phys. Rev. Appl.* **10**, (2018).

20. Lapine, M., Shadrivov, I. & Kivshar, Y. Wide-Band Negative Permeability of Nonlinear Metamaterials. *Sci. Rep.* **2**, 1–4 (2012).

21. Lin, K.-T., Lin, H., Yang, T. & Jia, B. Structured Graphene Metamaterial Selective Absorbers for High Efficiency and Omnidirectional Solar Thermal Energy Conversion. *Nat. Commun.* **11**, 1389 (2020).

22. Klotz, G., Malléjac, N., Guenneau, S. & Enoch, S. Controlling Frequency Dispersion in Electromagnetic Invisibility Cloaks. *Sci. Rep.* **9**, 6022 (2019).

23. Börsing, N. *et al.* Cloaking and Holography Experiments Using Immersive Boundary Conditions. *Phys. Rev. Appl.* **12**, 024011 (2019).

24. Zhang, M., Zhang, W., Liu, A. Q., Li, F. C. & Lan, C. F. Tunable Polarization Conversion and Rotation based on a Reconfigurable Metasurface. Sci. Rep. 7, 12068 (2017).

25. Soleymani, S., Güngördü, M. Z., Kung, P. & Kim, S. M. Ultra-High Efficiency and Broad Band Operation of Infrared Metasurface Anomalous Reflector based on Graphene Plasmonics. Sci. Rep. 9, 1249 (2019).

26. Zhang, H. et al. Multi-Functional Polarization Conversion Manipulation via

Graphene-based Metasurface Reflectors. Opt. Express 29, 70–81 (2021).

27. Baghel, A. K., Kulkarni, S. S. & Nayak, S. K. Linear-to-Cross-Polarization Transmission Converter Using Ultrathin and Smaller Periodicity Metasurface. IEEE Antennas Wirel. Propag. Lett. 18, 1433–1437 (2019).

28. Yuan, Y. et al. Independent Phase Modulation for Quadruplex Polarization Channels Enabled by Chirality-Assisted Geometric-Phase Metasurfaces. Nat. Commun. 11, 4186 (2020).

29. Baena, J. D., Glybovski, S. B., Del Risco, J. P., Slobozhanyuk, A. P. & Belov, P. A. Broadband and Thin Linear-to-Circular Polarizers Based on Self-Complementary Zigzag Metasurfaces. IEEE Trans. Antennas Propag. 65, 4124–4133 (2017).

30. Hao, J. et al. Manipulating Electromagnetic Wave Polarizations by Anisotropic Metamaterials. Phys. Rev. Lett. 99, 63908 (2007).

31. Phys, J. A. A Reconfigurable Ultra-Wideband Polarization Converter based on Metasurface Incorporated with PIN Diodes. J. Appl. Phys. 135105, (2019).

32. Jing, Y. et al. Achieving Circular-to-Linear Polarization Conversion and Beam Deflection Simultaneously using Anisotropic Coding Metasurfaces. Sci. Rep. 9, 12264 (2019).

33. Mun, S. E., Hong, J., Yun, J. G. & Lee, B. Broadband Circular Polarizer for Randomly Polarized Light in Few-Layer Metasurface. Sci. Rep. 9, 2543 (2019).

34. Gao, X. et al. A Reconfigurable Broadband Polarization Converter based on an

Active Metasurface. IEEE Trans. Antennas Propag. 66, 6086–6095 (2018).

35. Gansel, J. K. et al. Gold Helix Photonic Metamaterial as Broadband Circular Polarizer. Science 325, 1513-1515 (2009).

36. Wang, H. Bin, Cheng, Y. J. & Chen, Z. N. Wideband and Wide-Angle Single-Layered-Substrate Linear-to-Circular Polarization Metasurface Converter. IEEE Trans. Antennas Propag. 68, 1186–1191 (2020).

37. Yan, S. & Vandenbosch, G. A. E. Compact Circular Polarizer based on Chiral Twisted Double Split-Ring Resonator. Appl. Phys. Lett. 102, 103503 (2013).

38. Wu, S., Huang, X., Xiao, B., Jin, Y. & Yang, H. Multi-Band Circular Polarizer based on a Twisted Triple Split-Ring Resonator. Chinese Phys. B 23, 127805 (2014).

39. Cao, H. et al. Dual-Band Polarization Conversion based on Non-Twisted Q-Shaped Metasurface. Opt. Commun. 370, 311-318 (2016).

40. Xu, H., Wang, G., Qi, M., Cai, T. & Cui, T. Compact Dual-Band Circular Polarizer using Twisted Hilbert-Shaped Chiral Metamaterial. Opt. Express 21, 24912-24921 (2013).

41. Menzel, C., Rockstuhl, C. & Lederer, F. Advanced Jones Calculus for the Classification of Periodic Metamaterials. Phys. Rev. A. 82, 53811 (2010).

42. Shi, J. H., Ma, H. F., Guan, C. Y., Wang, Z. P. & Cui, T. J. Broadband Chirality and Asymmetric Transmission in Ultrathin 90° Twisted Babinet-Inverted Metasurfaces. Phys. Rev. B 89, 165128 (2014).

43. Zhao, J. & Cheng, Y. A High-Efficiency and Broadband reflective 90° Linear

Polarization Rotator based on Anisotropic Metamaterial. Appl. Phys. B 122, 255 (2016).

44. Liu, N., Mesch, M., Weiss, T., Hentschel, M. & Giessen, H. Infrared Perfect Absorber and its Application as Plasmonic Sensor. Nano Lett. 10, 2342–2348 (2010).